

# Synthesis and Characterization of Hierarchical NiO/Ni-Co-Mn Oxide Nanocomposite Materials for High Performance Supercapacitors

Ziyang Qin<sup>1</sup>, Ruidong Xu<sup>1,2,\*</sup>, Bohao Yu<sup>1</sup>, Wenbin Wang<sup>1</sup>, Ying Zhang<sup>1</sup>

<sup>1</sup> Faculty of Metallurgical and Energy Engineering, Kunming University of Science and Technology, Kunming 650093, China

<sup>2</sup> State Key Laboratory of Complex Nonferrous Metal Resources Clean Utilization, Kunming 650093, China

\*E-mail: [rdxupaper@aliyun.com](mailto:rdxupaper@aliyun.com)

Received: 28 August 2018 / Accepted: 12 October 2018 / Published: 7 February 2019

---

Hierarchical NiO/Ni-Co-Mn oxide nanocomposite materials on nickel foam substrates were prepared by chemical bath deposition. The elemental mappings, microstructures and phase structures were observed by field-emission scanning electron microscope and X-ray diffraction, and the electrochemical properties were measured by electrochemical workstation. The grid-like NiO nanosheets grew directly on nickel foam substrates, thereafter Ni-Co-Mn oxide nanosheets were coated on NiO nanosheets to form a layered composite structure. Cyclic voltammetry analysis shows that the obvious Faradaic reactions were found and the charge could be stored quickly. The low charge transfer resistance displays that the nanocomposite structure can improve the electrochemical activity. Meanwhile, the high specific capacity (1468.14 F g<sup>-1</sup> at a current density of 1 A g<sup>-1</sup>) and high cycle performance (90.76% retention at 5 A g<sup>-1</sup> after 3000 cycles) have been obtained by galvanostatic charge-discharge measurements. Therefore, NiO/Ni-Co-Mn oxide nanocomposite material as an ideal energy storage material may be potential to use in high performance supercapacitors.

---

**Keywords:** NiO nanosheets; Ni-Co-Mn oxide nanosheets; chemical bath deposition; hierarchical composite structure; supercapacitor

## 1. INTRODUCTION

As mainstream energy storage devices, supercapacitors and lithium batteries are widely used in many fields, including electric vehicles, power grids and portable personal electronics [1-2]. Supercapacitor has got more and more attention due to its high power density, fast charge and discharge, and long service life [3]. But, compared with lithium-ion batterie, lower energy density limits its use on a large scale [4]. In order to make up for these deficiencies, some researchers committed to the research

and development of new electrode materials, expecting to increase the specific capacity and extend the potential windows [5-6].

At present, the materials mainly used to prepare supercapacitors are carbon-based materials, transition metal oxides and conductive polymers [7-8]. Among them, transition metal oxides can store charge rapidly through Faradaic reactions on the surface of the electrodes [9]. At the same time, compared with carbon-based materials and conductive polymers, diversified crystal structure, higher specific capacity and cheaper price make transition metal oxides more attended [10]. Nickel oxide has become one of the most attractive electrode materials because of the high theoretical specific capacity, high electrochemical activity and low price [11]. The large scale ultrathin NiO nanoflake has been prepared by hydrothermal method, which possessed a specific capacity of  $870 \text{ mF cm}^{-2}$  at a current density of  $1 \text{ mA cm}^{-2}$  [12]. However, low electrical conductivity and poor mechanical properties restrict its real specific capacity and cycle life. These problems need to be solved urgently in order to play a greater role in the field of capacitors for nickel oxide [13].

In recent years, the polymetallic oxide has attracted wide attention due to the excellent conductivity. The oxides of Ni, Co and Mn have superior electrochemical properties, and their synergistic effect also can further improve other performances. For example, Ni-Co-Mn oxide nanosheet with a specific capacity of  $715.1 \text{ C g}^{-1}$  at a current density of  $1 \text{ A g}^{-1}$  have been obtained by chemical bath deposition and hydrothermal method [14]. Meanwhile, the structural design of the materials is also an important factor in improving the electrochemical performance. Compared with nanowires, nanotubes and nanoparticles, nanosheets are widely used due to their large specific surface areas [15-16]. In addition, the hierarchical composite structure has been widely concerned, which helps to improve the electrochemical properties and cyclic stability of the electrode materials [17].

In this study, hierarchical NiO/Ni-Co-Mn oxide nanocomposite materials on nickel foam substrates were prepared by chemical bath deposition. The elemental mappings, microstructures and phase structures were observed by field-emission scanning electron microscope and X-ray diffraction, and the electrochemical properties were measured by electrochemical workstation.

## 2. EXPERIMENTAL

All the chemical reagents were analytical grade in the experiments. Nickel foams were cut into small pieces ( $1 \times 2 \text{ cm}$ ), then soaked in hydrochloric acid and subjected to ultrasound for 30 minutes to remove the surface oxide layer. Thereafter, the clean nickel foams were washed several times with absolute ethanol and deionized water, placed in a vacuum drying oven and dried for 2 hours under  $60 \text{ }^\circ\text{C}$ .

### 2.1 Preparation of NiO nanosheets

$0.5 \text{ M NiSO}_4 \cdot 6\text{H}_2\text{O}$  and  $0.15 \text{ M K}_2\text{S}_2\text{O}_8$  were dissolved in  $40 \text{ ml}$  deionized water through magnetic stirring. Then the green clear solutions were placed in the water bath at  $50 \text{ }^\circ\text{C}$ . After 40 minutes, the pretreated nickel foams were put into the solution and  $4 \text{ ml}$  ammonia solution ( $25 \text{ wt\% NH}_3 \cdot \text{H}_2\text{O}$ ) was added to facilitate the reaction. Thereafter, the nickel foams were removed from the solution after

40 minutes and washed several times with deionized water. The precursors on nickel foam substrates were prepared and calcinated for 2 hours at 350 °C in the oven, and NiO nanosheets were obtained.

## 2.2 Preparation of Ni-Co-Mn oxide nanosheets

0.5 M NiSO<sub>4</sub>·6H<sub>2</sub>O, 0.5 M CoSO<sub>4</sub>·7H<sub>2</sub>O, 0.5 M MnSO<sub>4</sub>·H<sub>2</sub>O and 0.5 M K<sub>2</sub>S<sub>2</sub>O<sub>8</sub> were dissolved in 40ml deionized water. The clarified solutions were obtained through magnetic stirring and placed in the water bath at 50 °C. Then NiO nanosheets on the nickel foam substrates were put into the solution and 5 ml ammonia solution (25 wt% NH<sub>3</sub>·H<sub>2</sub>O) was added to facilitate the reaction. Thereafter, the nickel foams were removed from the solution after 40 minutes and washed several times with deionized water. The precursors of Ni, Co and Mn on nickel foam substrates were prepared and calcinated for 2 hours at 350 °C in the oven, and Ni-Co-Mn oxide nanosheets were obtained.

## 2.3. Material characterization

The microstructures were characterized by field-emission scanning electron microscope (FE-SEM, FEI Nova, NanoSEM 450). The phase structures were measured by powder X-ray diffraction (XRD, Rigaku D/Max-2200, Japan) using Cu Ka radiation from 10° to 80°.

## 2.4. Electrochemical measurements of materials

The electrochemical measurements were conducted in a three-electrode system with 2M KOH solution as electrolyte, in which the reference electrode was saturated calomel electrode (SCE), the counter electrode was Pt foil and the working electrodes were NiO nanosheets or Ni-Co-Mn oxide nanosheets on nickel foam substrates. Cyclic voltammetry (CV) and electrochemical impedance spectroscopy (EIS) were tested by an electrochemical workstation (Princeton, PARSTAT2273), the galvanostatic charge-discharge (GCD) and cycle life were carried out by CHI760E electrochemical workstation.

The specific capacity was calculated by the following formula [18]:

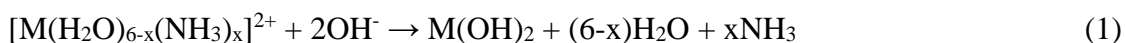
$$C=(I \cdot \Delta t)/(m \cdot \Delta V)$$

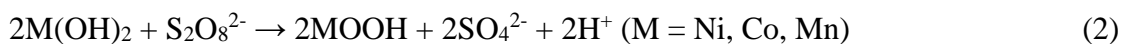
In which I is the discharge current, Δt is the discharge time, m is the quality of the active substance and ΔV is the voltage range.

## 3. RESULTS AND DISCUSSION

### 3.1. Chemical reaction and synthesis process

The formation of NiO and Ni-Co-Mn oxide nanosheets deposited on nickel foam substrates has almost the same forming process, and the possible corresponding reactions were shown as follows [19-22]:





During the course of chemical bath deposition, potassium persulfate was used as an oxidant for the reactions of Ni, Co and Mn ions. The metal hydroxide nanocrystals formed in the supersaturated solution were deposited on nickel foam substrates. Through these reactions, the overall surface energy can be reduced, and then these nanocrystals assembled and self-assembled to form the giant nanosheets. Finally, the metal hydroxyl oxide precursors were calcinated for 2 hours at 350 °C, and NiO/Ni-Co-Mn oxide nanocomposite materials on nickel foam substrates were obtained. Its synthesis diagram was shown in Figure 1.

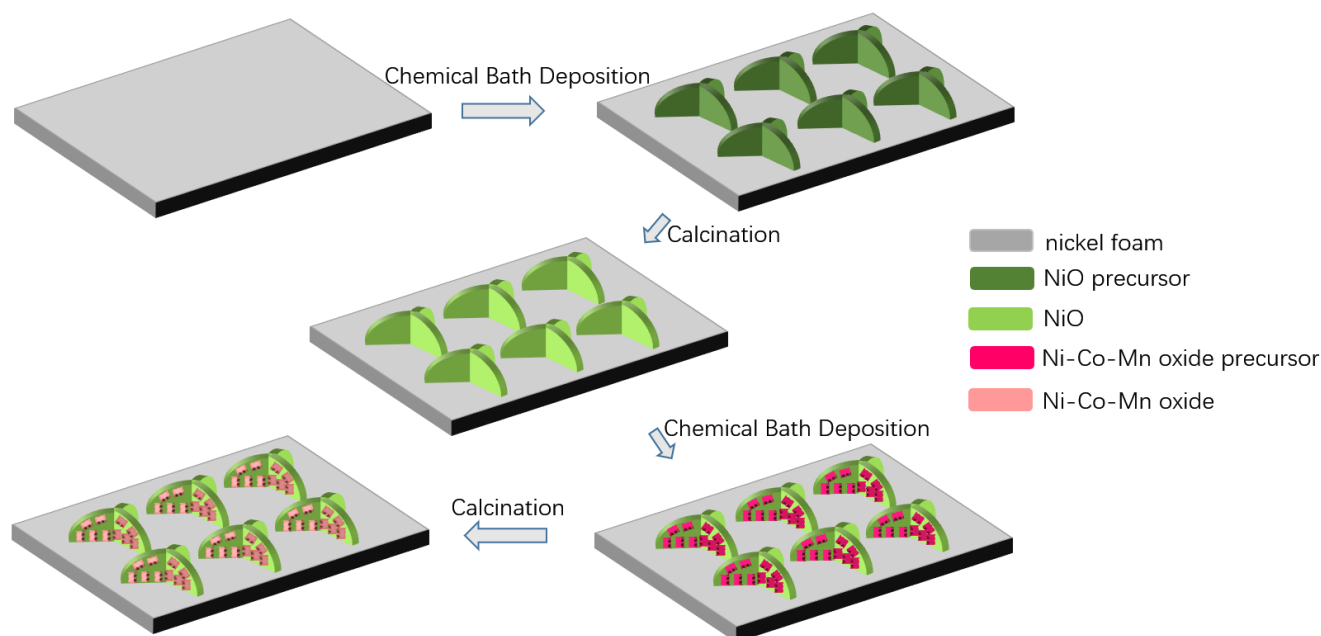


**Figure 1.** Schematic illustration for the synthesis process of the hierarchical NiO/Ni-Co-Mn oxide nanocomposite material on nickel foam substrate.

Therefore, Ni, Co and Mn oxide nanosheets can grow directly on nickel foam substrates, which make the materials possess good mechanical adhesion and electrical connection performance.

### 3.2. Microstructures and phase structures analysis

The FE-SEM images of the NiO nanosheet, Ni-Co-Mn oxide nanosheet and NiO/Ni-Co-Mn oxide nanocomposite material on nickel foam substrates were shown in Figure 2.

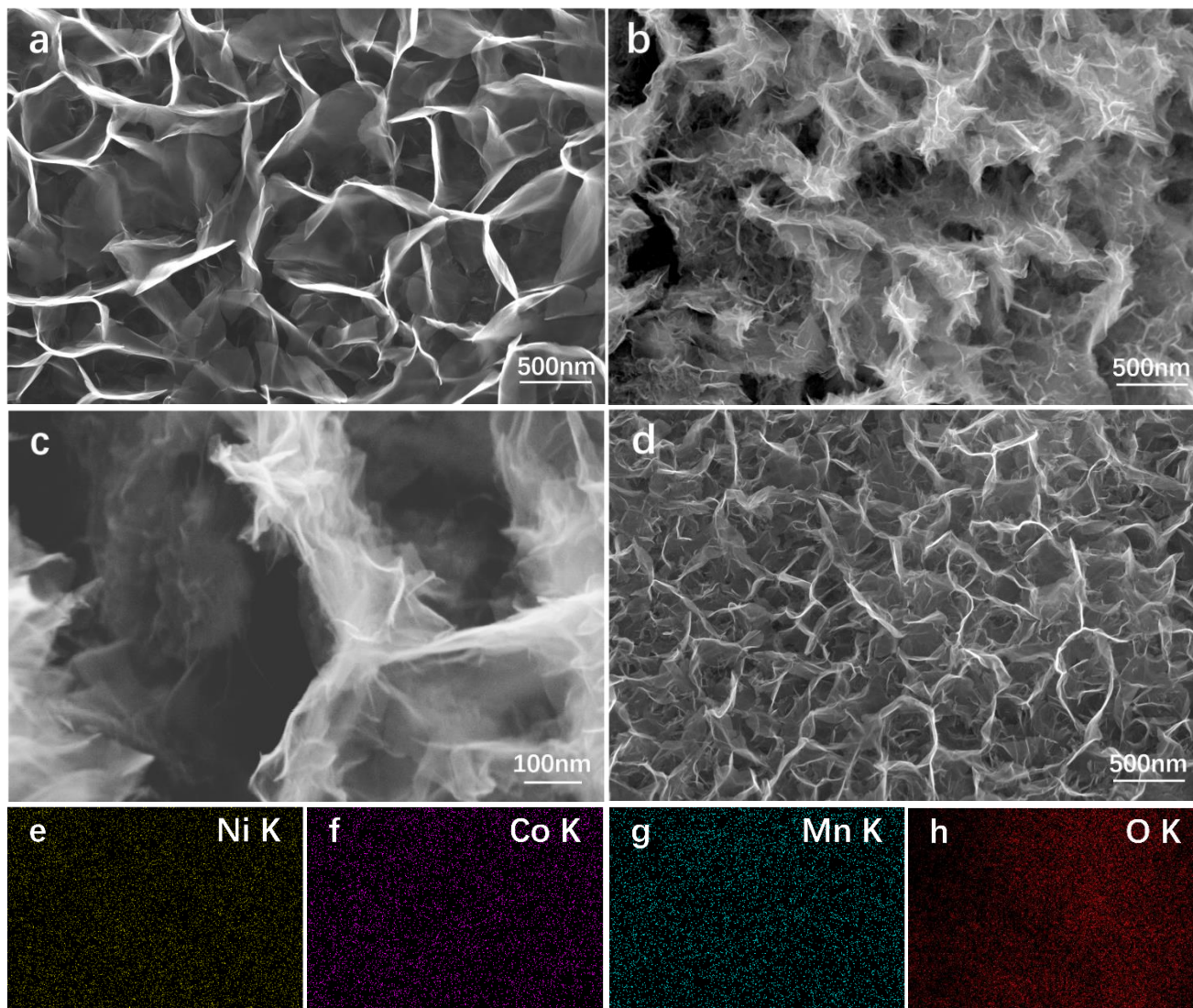


**Figure 2.** FE-SEM images of NiO nanosheet (a), NiO/Ni-Co-Mn oxide nanocomposite material (b, c) and Ni-Co-Mn oxide nanosheet (d), (e)-(h) showing elemental mappings for Ni, Co, Mn and O of image (d).

In Figure 2a, the NiO nanosheets with 400-1200 nm in length and 20-60 nm in thickness grew directly on nickel foam substrates and intersected with each other to form a complex grid structure. Meanwhile, the vertical growth of the nanosheets also greatly improved the surface areas of NiO. Based on this complex grid-like structure, NiO nanosheet has good structural stability and it is also possible to be used as the substrates for the growth of shell materials. After the second chemical bath deposition, a thin layer of Ni-Co-Mn oxide nanosheet with 15-30 nm in thickness as the shell was covered on the surface of the grid-shaped NiO nanosheets, as shown in Figure 2b and Figure 2c. In Figure 2c, it can be

seen that Ni-Co-Mn oxide nanosheet layers were thinly coated on the NiO nanosheet substrate framework. Compared with Figure 2b, Ni-Co-Mn oxide nanosheets directly deposited on nickel foam substrates were shown in Figure 2d. It is found from Figure 2d that Ni-Co-Mn oxide nanosheets on nickel foam substrates were also grid-shaped, but their sizes obviously increase. The main reason may be that the difference of the sedimentary substrate. Subjected to the sizes of NiO nanosheet substrates, the sizes of Ni-Co-Mn oxide nanosheets were smaller than those of one direction growth on nickel foam substrates. The size reduction that caused by this core-shell structure increased the surface areas and more loading mass also was obtained. Figure 2e-h shows the elemental mappings of Ni, Co, Mn and O, it is clear that Ni, Co and Mn existed and were uniformly distributed on the surface of NiO nanosheets.

Ni-Co-Mn oxide nanosheet and NiO/Ni-Co-Mn oxide nanocomposite material were stripped from the nickel foam surface and analyzed in order to avoid the influence of the substrate on phase structures, and their XRD patterns were shown in Figure 3.

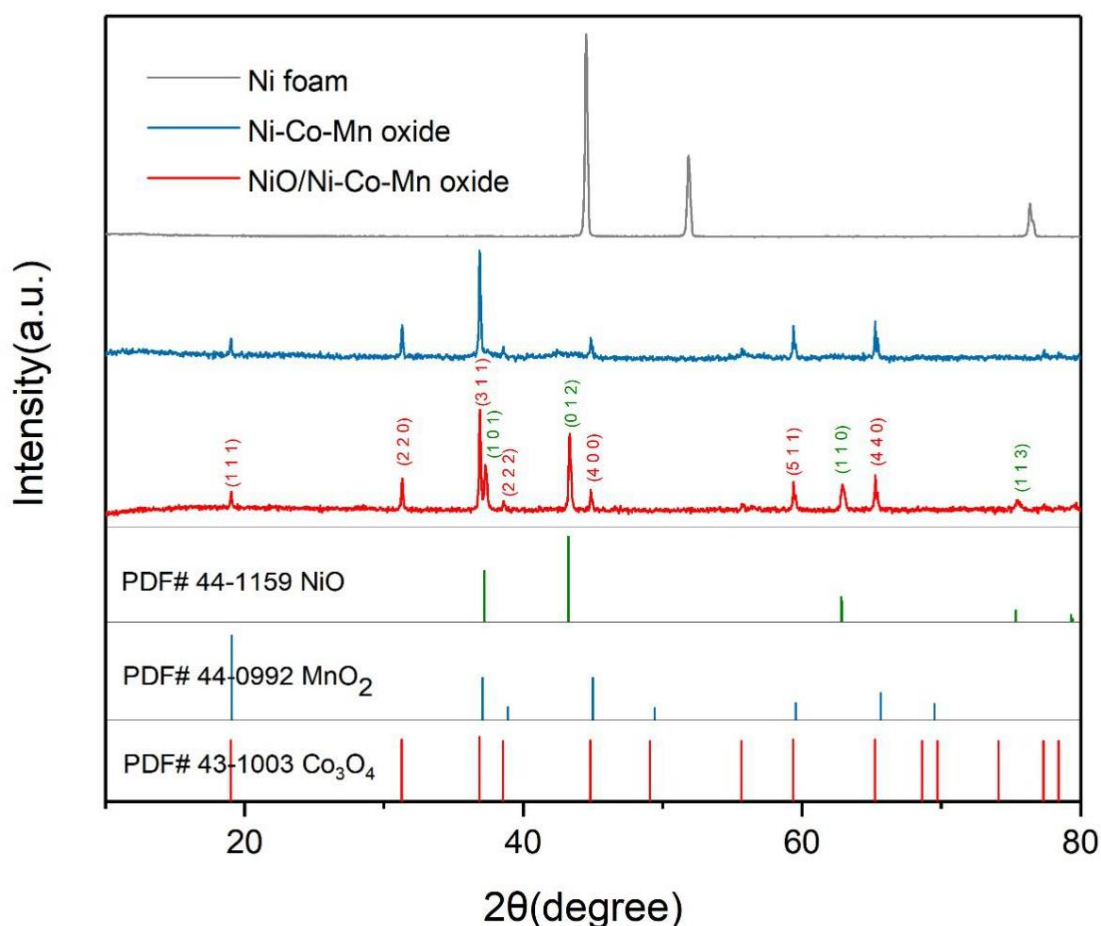


**Figure 3.** XRD patterns of nickel foam, Ni-Co-Mn oxide nanosheet and NiO/Ni-Co-Mn oxide nanocomposite material.

It can be seen from Figure 3 that the strong diffraction peaks were obtained at  $2\theta$  of  $37.25^\circ$ ,  $43.28^\circ$  and  $62.85^\circ$  in the structures of Ni-Co-Mn oxide nanosheet and NiO/Ni-Co-Mn oxide nanocomposite material, those were typical characteristic peaks of NiO (PDF No. 44-1159) at the (101), (012) and (110) crystal faces. In addition, there were other peaks at  $2\theta$  of  $31.27^\circ$ ,  $36.85^\circ$  and  $65.23^\circ$ , those were the peaks

of  $\text{Co}_3\text{O}_4$  (PDF No. 43-1003) at the (2 2 0), (3 1 1) and (4 4 0) crystal faces, indicating the generation of  $\text{Co}_3\text{O}_4$  on the nickel foam surfaces after that the precursors of Ni, Co and Mn were calcinated. In addition, there were no peaks of Ni and Mn in the diffraction pattern of Ni-Co-Mn oxide nanosheet, but Ni and Mn existed according to the Figure 2e-h, one possible reason is that Ni and Mn oxides were too little to be detected, another may be that Ni and Mn in the forms of ions replaced parts of Co atoms in the structure of  $\text{Co}_3\text{O}_4$  [23].

### 3.3. Electrochemical properties

Electrochemical properties of NiO nanosheet, Ni-Co-Mn oxide nanosheet and NiO/Ni-Co-Mn oxide nanocomposite material on nickel foam substrates were evaluated by CV, GCD and EIS, and the CV curves were shown in Figure 4.

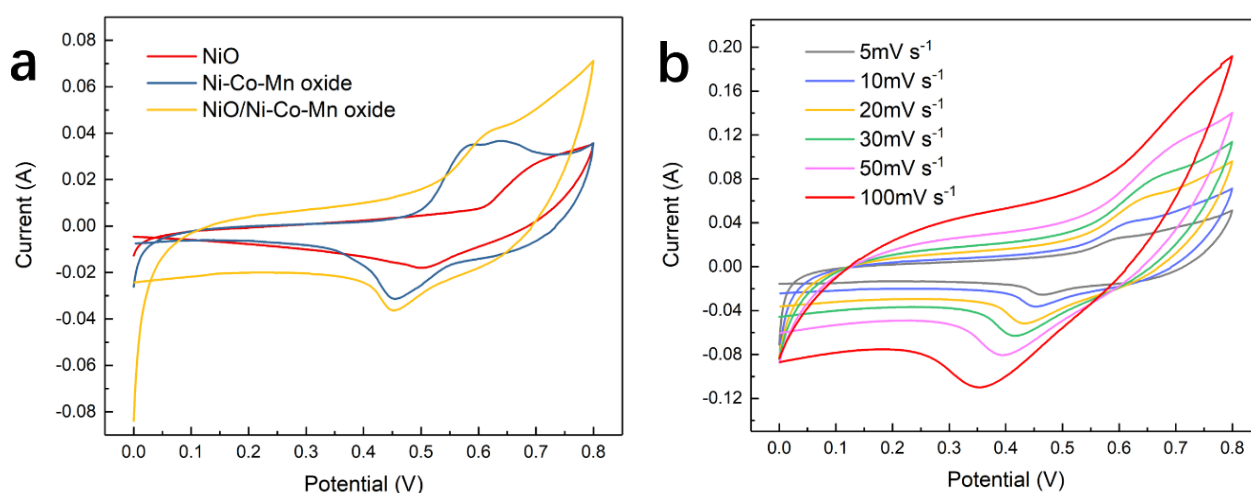


**Figure 4.** (a) CV curves of NiO nanosheet, Ni-Co-Mn oxide nanosheet and NiO/Ni-Co-Mn oxide nanocomposite material at a constant scan rate  $10 \text{ mV s}^{-1}$ , (b) CV curves of NiO/Ni-Co-Mn oxide nanocomposite material at various scan rate from 5 to  $100 \text{ mV s}^{-1}$ .

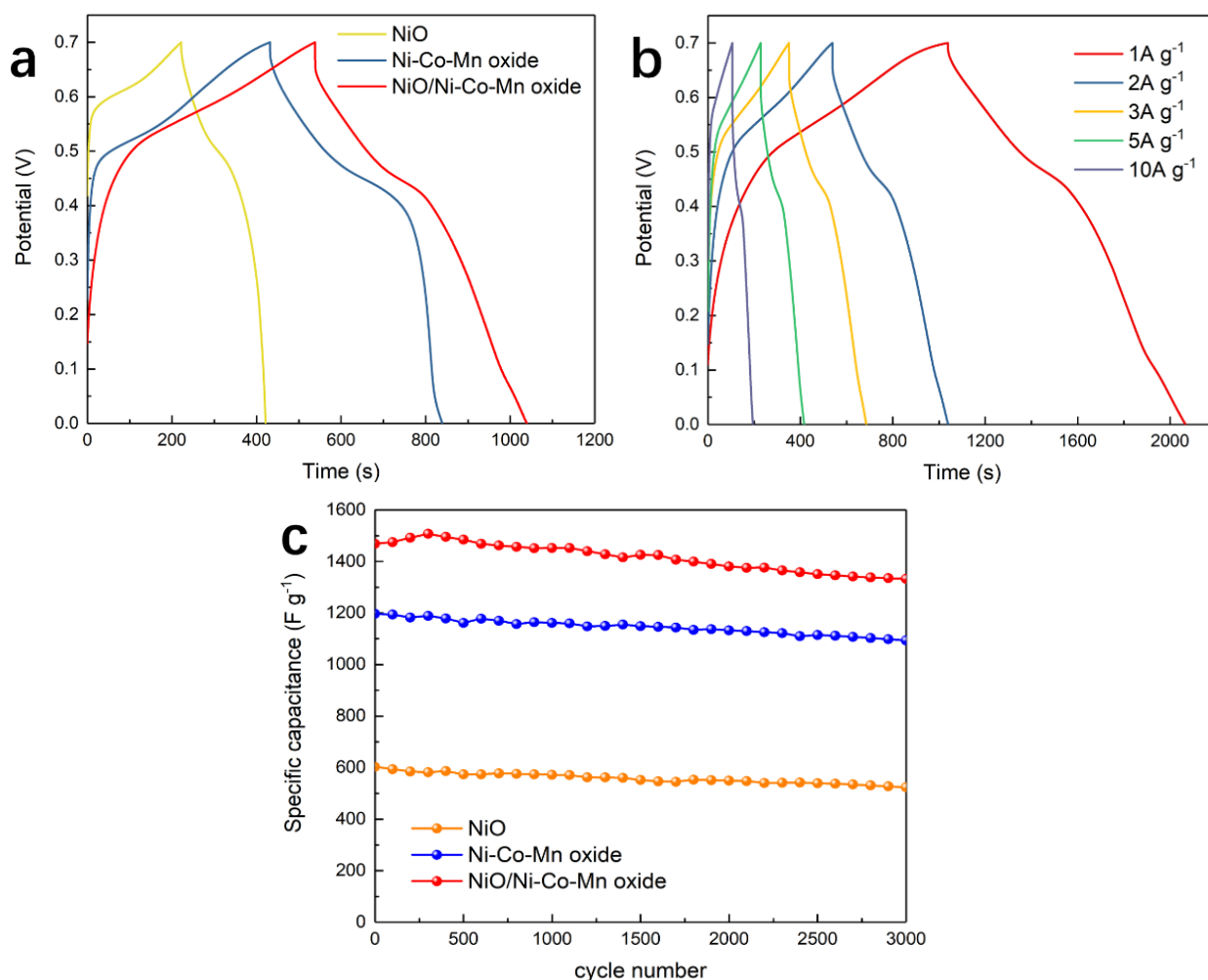
Figure 4a is a comparison of CV curves for the NiO nanosheet, Ni-Co-Mn oxide nanosheet and NiO/Ni-Co-Mn oxide nanocomposite material under a potential window of 0-0.8 V. The redox peaks appeared in three locations. Those peaks exhibited obvious battery characteristics, so the CV curves were different from the rectangular those of the general electric double-layer capacitors. The anodic peak potentials of NiO nanosheet, Ni-Co-Mn oxide nanosheet and NiO/Ni-Co-Mn oxide nanocomposite material were around 0.67, 0.57 and 0.61 V, and their cathodic peak potentials were around 0.51, 0.45 and 0.44 V. It can be seen that the redox current of NiO/Ni-Co-Mn oxide nanocomposite material was higher than that of NiO nanosheet and Ni-Co-Mn oxide nanosheet. The largest area indicated that NiO/Ni-Co-Mn oxide nanocomposite material had the highest specific capacity.

Figure 4b displays the CV curves of NiO/Ni-Co-Mn oxide nanocomposite material at different scan rates. It is obvious that the distinct redox peaks were produced between the active materials and

electrolytes, exhibiting a pure Faradaic performance [24]. The Faradaic redox reactions in an alkaline electrolyte were expressed as follows [25]:



The above CV curves at different scan rates can reflect the conductivity of the materials. It can also be seen from Figure 4b that the oxidation peaks gradually turned into spindle shape with increasing scanning rate from 5 to 100 mV s<sup>-1</sup>. The main reason is that ions and electrons can only contact finite outer surface and not enter into the internal structure at high scanning rates [26].



**Figure 5.** (a) GCD curves of NiO nanosheet, Ni-Co-Mn oxide nanosheet and NiO/Ni-Co-Mn oxide nanocomposite material, (b) GCD curves of NiO/Ni-Co-Mn oxide nanocomposite materials under different current densities, (c) The cycle performance of NiO nanosheet, Ni-Co-Mn oxide nanosheet and NiO/Ni-Co-Mn oxide nanocomposite material.

The GCD measurements were conducted under a potential window of 0–0.7 V, and the results were shown in Figure 5.

Figure 5a shows the GCD curves of NiO nanosheet, Ni-Co-Mn oxide nanosheet and NiO/Ni-Co-Mn oxide nanocomposite material at a current density of 2 A g<sup>-1</sup>. It can be seen from Figure 5a that these curves reflected the existence of redox reactions, which were consistent with CV curves. All three GCD curves had obvious nonlinear characteristics, indicating that the specific capacity was mainly produced by Faradaic reactions rather than the electric double layer energy storage. Moreover, the specific capacities of NiO nanosheet, Ni-Co-Mn oxide nanosheet and NiO/Ni-Co-Mn oxide nanocomposite material were 571.43, 1162.86, and 1431.53 F g<sup>-1</sup>, respectively. Among three materials, the specific capacity of NiO/Ni-Co-Mn oxide nanocomposite material was the highest, which is good for improving the electrochemical activity and specific capacity.

Figure 5b shows the GCD curves of NiO/Ni-Co-Mn oxide nanocomposite materials under different current densities from 1 to 10 A g<sup>-1</sup>. The specific capacities of 1, 2, 3, 5, 10 A g<sup>-1</sup> were 1468.14, 1431.53, 1391.62, 1344.67 and 1270.34 F g<sup>-1</sup>, respectively. It is found that with the increase of the current density, the discharge platform was gradually shortened and the discharge amount was gradually decreased. The specific capacity was decreased with the increase of current density may be that the diffusion of OH<sup>-</sup> ions in the electrolyte was too slow to meet the needed amount of OH<sup>-</sup> ions on the surface of the electrode under the condition of high current density [27].

The cycling performance of NiO nanosheet, Ni-Co-Mn oxide nanosheet and NiO/Ni-Co-Mn oxide nanocomposite material was measured by GCD under the current density of 5 A g<sup>-1</sup>, as shown in Figure 5c. It is obvious that the specific capacity retention rate of NiO/Ni-Co-Mn oxide nanocomposite material remained at 90.76%, showing good circulation performance after 3000 cycles.

The specific capacity performance of several types of composite materials was listed in Table 1, containing Ni-Co-Mn oxide, Co<sub>3</sub>O<sub>4</sub>/MnO<sub>2</sub>, Co<sub>3</sub>O<sub>4</sub>/MnO<sub>2</sub>–NiO/Co<sub>3</sub>O<sub>4</sub>/MnO<sub>2</sub>, MnO<sub>2</sub>/NiCo<sub>2</sub>O<sub>4</sub> and NiO/Ni-Co-Mn oxide. It can be seen from Table 1 that NiO/Ni-Co-Mn oxide nanocomposite material obtained in this research possessed a higher specific capacity than other composite materials, indicating that as an ideal energy storage material, NiO/Ni-Co-Mn oxide nanocomposite material on nickel foam substrate may be potential to use in high performance supercapacitors.

**Table 1.** Comparison of the specific capacity performance of several types of composite materials

Material	Morphology	Method	Specific capacity (F g <sup>-1</sup> )	Reference
Ni-Co-Mn oxide	nanotubes	Hydrothermal	680	[28]
Ni-Co-Mn oxide	nanoflakes	Microwave synthesis	1151	[29]
Co <sub>3</sub> O <sub>4</sub> /MnO <sub>2</sub>	microspheres	Hydrothermal	671	[30]
NiO/Co <sub>3</sub> O <sub>4</sub> /MnO <sub>2</sub>	nanosheets	Hydrothermal	792.5	[31]
MnO <sub>2</sub> /MnCo <sub>2</sub> O <sub>4</sub>	nanoparticles	Solution combustion	497	[32]
MnO <sub>2</sub> /NiCo <sub>2</sub> O <sub>4</sub>	nanospheres	Microemulsion method	1127.27	[33]
NiCo <sub>2</sub> O <sub>4</sub> /MnO <sub>2</sub>	nanosheets	Electrodeposition	913.6	[34]
NiO/Ni-Co-Mn oxide	nanosheets	Chemical bath deposition	1468.14	This work

In order to further understand the charge conduction performance, the EIS of NiO nanosheet, Ni-Co-Mn oxide nanosheet and NiO/Ni-Co-Mn oxide nanocomposite material was measured, and their Nyquist plots in the frequency range of 100 kHz to 0.1 Hz were shown in Figure 6.

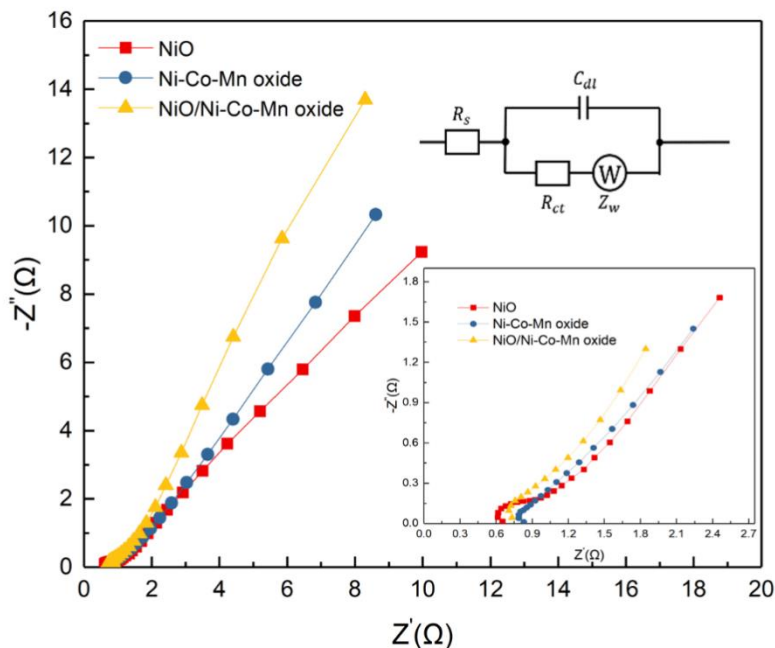


**Figure 6.** The Nyquist plots of NiO nanosheet, Ni-Co-Mn oxide nanosheet and NiO/Ni-Co-Mn oxide nanocomposite material. Inset: the zoom-in Nyquist plots at the high-frequency region and the electrical equivalent circuit used for fitting impedance spectra.

The impedance spectrum is consisted of the curve of the high-frequency region of the charge-transfer resistance ( $R_{ct}$ ) and the straight line of the low-frequency zone representing Warburg impedance ( $Z_w$ ) [35]. Meanwhile, the intercept of Nyquist plots on the X-axis represents the internal resistance ( $R_s$ ), including intrinsic resistance of substrate, ionic resistance of electrolyte and contacting resistance between active materials and current collector interface [36]. According to the equivalent circuit diagram shown in Figure 6, it is known by fitting analysis that the  $R_s$  of NiO nanosheet, Ni-Co-Mn oxide nanosheet and NiO/Ni-Co-Mn oxide nanocomposite material were 0.62  $\Omega$ , 0.84  $\Omega$  and 0.75  $\Omega$ , respectively. The  $R_{ct}$  of NiO/Ni-Co-Mn oxide nanocomposite material was 0.15  $\Omega$ , which was significantly less than 0.28  $\Omega$  of NiO nanosheet and 0.17  $\Omega$  of Ni-Co-Mn oxide nanosheet. The low  $R_{ct}$  is beneficial to Faradaic reaction, so NiO/Ni-Co-Mn oxide nanocomposite material shows higher electrochemical activity and specific capacity [37].

#### 4. CONCLUSIONS

Hierarchical NiO/Ni-Co-Mn oxide nanocomposite materials on nickel foam substrates have been prepared by chemical bath deposition and calcination. The grid-like NiO nanosheets grew directly on nickel foam substrates, thereafter Ni-Co-Mn oxide nanosheets were coated on the NiO nanosheets to

form a layered composite structure. NiO/Ni-Co-Mn oxide nanocomposite material exhibited high specific capacity of  $1468.14 \text{ F g}^{-1}$  at a current density of  $1 \text{ A g}^{-1}$ , high cycle performance of 90.76% retention at  $5 \text{ A g}^{-1}$  after 3000 cycles and low charge-transfer resistance of  $0.15 \Omega$ . Therefore, it may be potential to use in high performance supercapacitors.

#### ACKNOWLEDGMENTS

Authors gratefully acknowledge the financial supports of the National Natural Science Foundation of China (Project No. 51874154); the Key Project of Yunnan Province Applied Basic Research Plan of China (Project No. 2014FA024); the Specialized Research Fund for the Doctoral Program of the Ministry of Education of China (Project No. 20125314110011).

#### References

1. P. Simon and Y. Gogotsi, *Nat. Mater.*, 7 (2008) 845.
2. X. Peng, L. Peng, C. Wu and Y. Xie, *Chem. Soc. Rev.*, 43 (2014) 3303.
3. Y. Luo, H. Zhang, L. Wang, M. Zhang and T. Wang, *Electrochim. Acta*, 180 (2015) 983.
4. L. Hao, X. Li and L. Zhi, *Adv. Mater.*, 25 (2013) 3899.
5. G. Wang, L. Zhang and J. Zhang, *Chem. Soc. Rev.*, 41 (2012) 797.
6. P.C. Chen, G. Shen, Y. Shi, H. Chen and C. Zhou, *ACS nano*, 4 (2010) 4403.
7. C.R. Mariappan, S. Upadhyay, V. Kumar, S. Indris and H. Ehrenberg, *Ceram. Int.*, 44 (2018) 8864.
8. G. Rajeshkhanna and G.R. Rao, *Electrochim. Acta*, 261 (2018) 265.
9. U.M. Patil, R.R. Salunkhe, K.V. Gurav and C.D. Lokhande, *Appl. Surf. Sci.*, 255 (2008) 2603.
10. W. Deng, X. Ji, Q. Chen and C.E. Banks, *RSC Adv.*, 1 (2011) 1171.
11. J.M. Xu, K.Y. Ma and J.P. Cheng, *J. Alloys Compd.*, 653 (2015) 88.
12. H. Xiao, F. Qu and X. Wu, *Appl. Surf. Sci.*, 360 (2016) 8.
13. D. Cheng, Y. Yang, Y. Luo, C. Fang and J. Xiong, *Electrochim. Acta*, 176 (2015) 1343.
14. S. Chen, G. Yang and H. Zheng, *Electrochim. Acta*, 220 (2016) 296.
15. A. Paravannoor, R. Ranjusha, A.M. Asha, R. Vani, S. Kalluri, K.R.V. Subramanian, N. Sivakumar, T.N. Kim, S.V. Nair and A. Balakrishnan, *Chem. Eng. J.*, 220 (2013) 360.
16. Z. Zhu, J. Ping, X. Huang, J. Hu, Q. Chen, X. Ji and C.E. Banks, *J. Mater. Sci.*, 47 (2012) 503.
17. X. Bai, Q. Liu, J. Liu, H. Zhang, Z. Li, X. Jing, P. Liu, J. Wang and R. Li, *Chem. Eng. J.*, 315 (2017) 35.
18. M. Pang, G. Long, S. Jiang, Y. Ji, W. Han, B. Wang, X. Liu and Y. Xi, *Electrochim. Acta*, 161 (2015) 297.
19. X.H. Xia, J.P. Tu, J. Zhang, X.L. Wang, W.K. Zhang and H. Huang, *Sol. Energ. Mat. Sol. C.*, 92 (2008) 628.
20. D. Chen, F. Giroud and S.D. Minteer, *J. Electrochem. Soc.*, 161 (2014) F933.
21. M. Figlarz, J. Guenot and F. Fievet-Vincent, *J. Mater. Sci.*, 11 (1976) 2267.
22. G. Xi, Y. Peng, Y. Zhu, L. Xu, W. Zhang, W. Yu and Y. Qian, *Mater. Res. Bull.*, 39 (2004) 1641.
23. L. Li, Y. Zhang, F. Shi, Y. Zhang, J. Zhang, C. Gu, X. Wang and J. Tu, *ACS Appl. Mater. Interfaces*, 6 (2014) 18040.
24. K.Y. Ma, F. Liu, M.B. Zhang, X.B. Zhang and J.P. Cheng, *Electrochim. Acta*, 225 (2017) 425.
25. L. Li, Y.Q. Zhang, X.Y. Liu, S.J. Shi, X.Y. Zhao, H. Zhang, X. Ge, G.F. Cai, C.D. Gu, X.L. Wang and J.P. Tu, *Electrochim. Acta*, 116 (2014) 467.
26. Y.X. Zhang, M. Kuang, X.D. Hao, Y. Liu, M. Huang, X.L. Guo, J. Yan, G.Q. Han and J. Li, *J. Power Sources*, 270 (2014) 675.
27. J.J. Zhou, M.K. Wu, K. Tao, Y.L. Li, Q. Li, C. Chen, F.Y. Yi and L. Han, *J. Alloys Compd.*, 748 (2018) 496.
28. H. Wang, Y. Fu, X. Wang, J. Gao, Y. Zhang and Q. Zhao, *J. Alloys Compd.*, 639 (2015) 352.
29. C. Lamiel, V.H. Nguyen, D.R. Kumar and J.J. Shim, *Chem. Eng. J.*, 316 (2017) 1091.

30. H. Che, Y. Lv, A. Liu, J. Mu, X. Zhang and Y. Bai, *Ceram. Int.*, 43 (2017) 6054.
31. H. Wang, Q. Ren, D.J.L. Brett, G. He, R. Wang, J. Key and S. Ji, *J. Power Sources*, 343 (2017) 76.
32. Y. Zhang, H. Xuan, Y. Xu, B. Guo, H. Li, L. Kang, P. Han, D. Wang and Y. Du, *Electrochim. Acta*, 206 (2016) 278.
33. Y. Zhou, L. Ma, M. Gan, M. Ye, X. Li, Y. Zhai, F. Yan and F. Cao, *Appl. Surf. Sci.*, 444 (2018) 1.
34. Y. Zhang, B. Wang, F. Liu, J. Cheng, X. Zhang and L. Zhang, *Nano Energy*, 27 (2016) 627.
35. X. Tian, C. Cheng, L. Qian, B. Zheng, H. Yuan, S. Xie, D. Xiao and M.M.F. Choi, *J. Mater. Chem.*, 22 (2012) 8029.
36. M.S. Wu, C.Y. Huang and K.H. Lin, *J. Power Sources*, 186 (2009) 557.
37. Y.F. Yuan, J.X. Lin, D. Zhang, S.M. Yin, Y.L. Zhao, J.L. Yang, Y.B. Chen and S.Y. Guo, *Electrochim. Acta*, 227 (2017) 303.

© 2019 The Authors. Published by ESG ([www.electrochemsci.org](http://www.electrochemsci.org)). This article is an open access article distributed under the terms and conditions of the Creative Commons Attribution license (<http://creativecommons.org/licenses/by/4.0/>).